Engineering Geology 352 (2025) 108073

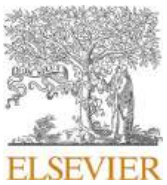

Contents lists available at ScienceDirect

Engineering Geology

journal homepage: www.elsevier.com/locate/enggeo

A three-dimensional agro-hydrological model for predictive analysis of shallow landslides: CRITERIA-3D

G. Sannino [a,b,*], F. Tomei [a], M. Bittelli [c], C. Meisina [d], M. Bordoni [d], R. Valentino [b]

[a] Regional Agency for Prevention, Environment and Energy of Emilia-Romagna Region, Bologna, Italy
[b] Department of Chemistry, Life Sciences and Environmental Sustainability, University of Parma, Parma, Italy
[c] Department of Agricultural and Food Sciences, University of Bologna, Bologna, Italy
[d] Department of Earth and Environmental Sciences, University of Pavia, Pavia, Italy

ARTICLE INFO

Keywords:
Shallow landslides modeling
Soil hydrological balance
Crop development
Slope stability
Physically-based modeling
Digital Elevation Model

ABSTRACT

In this paper a three-dimensional agro-hydrological model for shallow landslides' prediction is presented. The model is an extension of the CRITERIA-3D free-source model for crop development and soil hydrology, developed by the Hydrometeorological service of the Regional Agency for Environmental prevention and Energy of Emilia-Romagna region (Arpae-simc). The soil-water balance is computed through the coupling of surface and sub-surface flows in multi-layered soils over areas topographically characterized by Digital Elevation Model (DEM). The rainfall infiltration process is simulated through a three-dimensional version of Richards' equation. Surface runoff, lateral drainage, capillarity rise, soil evaporation and plant transpiration contribute to the computation of the soil hydrology on an hourly basis. The model accepts meteorological hourly records as input data and outputs can be obtained for any time step at any selected depth of the soil profile. Among the outputs, volumetric water content, soil-water potential and the factor of safety of the slope can be selected. The validation of the proposed model has been carried out considering a test slope in Montuè (northern Italy), where a shallow landslide occurred in 2014 a few meters away from a meteorological and soil moisture measurement station. The paper shows the accuracy of the model in predicting the landslide occurrence in response to rainfall both in time and space. Although there are some model limitations, at the slope scale the model results are highly accurate with respect to field data even when the spatial resolution of the Digital Elevation Model is reduced.

1. Introduction

Rainfall-induced shallow landslides and erosion are widespread phenomena that affect people and territories. Future projections show that global warming, because of the rise in temperatures, will increase the extreme rainfall events worldwide (IPCC, 2023). Extreme events can provoke shallow landslides with high probability in those territories that already present a series of predisposing factors. Shallow landslides, although involving small volumes of soil, represent a hazard since they don't show premonitory signs over territories (Persichillo et al., 2017). Sometimes the material involved provokes a rapid evolution in debris or earth flows moving at very high velocities. Beyond the specific evolution of the phenomenon, a single extreme rainfall event over landslide-prone territories may cause a dense distribution of landslides (Bordoni et al., 2015). Tools that can detect in advance the location and timing of landslide occurrence are of high importance, especially in countries that are hotspots for landslide hazard in Europe. Italy is a particular country of interest, being the first country in Europe for the number of landslide events (Guzzetti et al., 1999). Although some confusion exists in literature, hazard landslide assessment is defined as the probability of instability occurring within a given area and in a given period of time. It means defining "when" or "how frequently" a certain kind of landslide will occur (Reichenbach et al., 2018).

Extreme climatic events are arising, and some of them are very destructive. An example is the May 2023 flood occurred in Emilia-Romagna region, where 65′598 shallow landslides were triggered and 78.5 % of them occurred in areas that were not included in available landslide inventories (Brath et al., 2023). In fact, although most of the landslide prediction techniques have been based on the assumption of the stationarity of rainfall events, (i.e., considering that "the past is a guide for the future" as discussed by Guzzetti et al., 2020), this condition is not anymore guaranteed under climate change forcings. Moreover, it

* Corresponding author.
E-mail address: giada.sannino@unipr.it (G. Sannino).

https://doi.org/10.1016/j.enggeo.2025.108073
Received 19 November 2024; Received in revised form 2 April 2025; Accepted 7 April 2025
Available online 11 April 2025

is difficult to precisely detect the triggering time of a landslide during a precipitation event. In this perspective, physically-based tools for modeling processes acting at both surface and subsurface levels are of importance (Anagnostopoulos et al., 2015). More particularly, the landslide occurrence constitutes the final step of a chain of processes that starts from the rainfall event and leads to the loss of the strengthening effect exerted by soil suction, and early warning systems should take into account the singular components in order to be used as real-time analysis tools (Olivares et al., 2014). Determining a-priori when the triggering moment will be reached, especially at distributed scales, is an ambitious task that is only partially solved by empirical methods such as the adoption of rainfall thresholds (Tiranti and Rabuffetti, 2010; Papa et al., 2013; Bordoni et al., 2019).

Physically-based methods, at the cost of major consumption of computational time and energy, constitute a flexible tool. In fact, when applied at large scales, physically-based models can account for several different transient processes when representing reality. This ability is not guaranteed by statistical or empirical methods, and the literature reports different examples of merging these two complementary approaches (Oliveira et al., 2017; Park et al., 2019; Hwang et al., 2023).

Storically, landslide detection methods have been based on saturated soil conditions, adopting the Terzaghi's effective stress principle, in which suction is quantified through saturated seepage theories (Lu and Godt, 2008; Gofar and Rahardjo, 2017). Although these methods obtain conservative measures of slope stability as they mostly consider restrictive assumptions (i.e., the soil is saturated, the water potential is positive and thus the soil strength is at its minimum value) they may not be accurate for practical landslide hazard assessment. In fact, they appear not suitable to be adopted for near-real time landslides' detection tools such as early warning systems, where the consideration of transient suction effects is of high importance (Fredlund, 1987; Godt et al., 2012). During some field monitoring campaigns, different landslides have been observed to occur even when the soil was still in partially saturated condition, that is more likely to occur meanwhile a rainfall event is ongoing, as water content and pore water pressure changes affect the soil strength (Toll et al., 2011). Only through physically-based models that consider unsaturated soil mechanics the triggering of such landslides can be predicted. Anyhow, especially when the soil moisture is high due to antecedent precipitation events, the saturation condition may be reached during the triggering rainfall event. Thus, when assessing slope stability, including initial or antecedent moisture conditions can raise the prediction accuracy and be a valid tool for civil protection purposes (Greco et al., 2023). For the same reasons, as vegetation affects the soil water conditions, the modeling of its effects on both soil hydrological behavior and stability is an aspect that should be considered (Gonzalez-Ollauri and Mickovski, 2017a; Sannino et al., 2024), although it is still under debate if after heavy storms these effects are exerted or not (Zhang et al., 2022; Masi et al., 2023). Nonetheless, predictive slope stability analyses of shallow landslides often neglect vegetation reinforcement effects, which are not completely explored yet.

It is known that physically-based models can account for the above-mentioned aspects in slope stability computation, as they can quantify specific effects and their relative importance (Corominas et al., 2014). Physically-based models for triggering mechanisms of shallow landslides can give insights in landslide formation, delivering decision-makers deeper points of view for taking action and prevention measurements.

At a regional or watershed scale, the use of three-dimensional hydrological models provides realistic representation of soil conditions prior and during rainfall events, leading to an improvement in both space and time forecasting capabilities (Simoni et al., 2008). This is especially due to the possibility of modeling lateral redistribution processes and not only the vertical upward or downward water movements, as one-dimensional models do (Bogaard and Greco, 2016). Moreover, three-dimensional models can consider complex topography that in most cases constitutes an important predisposing factor for shallow landslides (Fernandes et al., 2004).

Normally, landslide hazard assessment models are composed by an hydrological module interconnected with a geotechnical one (DiBiagio et al., 2024). The landslide hazard assessment in three-dimensional distributed models can be computed either considering stationary or transient hydrology. In this latter case, rainfall input over the spatial domain is a dynamic variable, which represents the real temporal pattern of rainfall. When the distributed model is related to very large areas, rainfall inputs should also be spatially interpolated based on real rainfall gauge records; in fact, evidence showed that the landslide spatial patterns are linked to the precipitation spatio-temporal resolution (Hong et al., 2006).

A further component that affects shallow landslides and can be modeled based on real meteorological data is the vegetation growth (McMaster and Wilhelm, 1997). Such an aspect can constitute an advisable tool in relation to climate change adaptation strategies (Wypych et al., 2017). In fact, under climate change forcing, environmental conditions and their effect on the vegetation could not be accurately represented if a stationary plant coverage is adopted, especially because vegetation responses to climate are non-static components of the hydrological balances (Martin, 1993). The possibility of simulating roots and canopies dynamically can raise the insights provided by a model simulation.

As it is well known, vegetation effects on slope stability have been studied in detail in the last decades (Murgia et al., 2022). However, not only the vegetation should be modeled as changing with time, but also its properties should be able to change together with the soil moisture and rainfall conditions (Gonzalez-Ollauri and Mickovski, 2017b).

Most of the three-dimensional distributed models adopt a unique, comprehensive soil water balance (SWB) equation comprising selected hydrological processes, such as the infiltration, which is commonly simulated through Richards' equation (Van Dam and Feddes, 2000). The use of Richards' equation implies that the soil is considered as an homogeneous porous medium; indeed, soil properties and structure are not spatially homogeneous (Young et al., 2001; Zuo et al., 2009). A source of spatial heterogeneity related to soil water flow is the presence of macro voids and preferential paths, through which water bypasses a large part of the soil matrix (Hagedorn and Bundt, 2002). When drying, fine-grained soils can undergo the formation of soil cracking of different depths and widths, which constitute a typology of macro voids (Peron et al., 2009). Soil cracking process is a complex phenomenon, although the flow behavior through them and their evolution has been characterized by several studies (e.g. Krisnanto et al., 2014; Stewart and Najm, 2020; Zhang et al., 2021; Luo et al., 2023). It is known that the amount of clay content promotes the crack formation, but crack formation in vegetated soil structures is still only partially explored (Tang et al., 2021). It was shown that capillary forces resulting from soil drying can cause shrinkage and suction in soil mass (Tang et al., 2011) and can induce cracks formation as consequence (Fredlund and Rahardjo, 1993; Safari et al., 2014). Involving complex soil hydrological processes such as the macropores flow in shallow landslide triggering models could help in landslide prediction.

In literature, different attempts have demonstrated the benefits of considering the topography effects on soil water balance, especially when lateral flows are considered (Lepore et al., 2013). Instead, the vegetation effects on either hydrology or slope stability are rarely considered, unless they are assumed as a constant additional mechanical term of global soil cohesion. Even considering specific characteristics such as root morphological attributes to determine vegetation effects on the stability of a single slope is quite common; however, it is difficult to extend these effects over large-scale analyses, especially because the repeated collection of sample data is labor-intensive (Liu et al., 2022). On the other hand, adopting a unique value of any parameter related to vegetation for long-term simulations does not represent the reality, and a physical, transient model is an effective way to derive a consistent approximation of real ecology over large areas. In the literature, models

such as GEOtop-FS (Rigon et al., 2006; Simoni et al., 2008) or TRIGRS (Baum and Godt, 2008) are considered to be among the most advanced existing physically-based tools (Meena et al., 2022), as they consider simultaneously a three-dimensional hydrology and spatially variable soil characteristics. However, models that simultaneously consider soil stratigraphy, spatial variability, complex three-dimensional hydrology and transient modeling of vegetation - in both canopies and roots - based on real meteorological conditions, are still rare.

An aspect that is rarely addressed when hydrological models are developed is the effect that the spatial resolution of input data may have on the outputs. More particularly, the Digital Elevation Model (DEM), which usually defines the mesh of the model computation, has been demonstrated to have an effect on numerical models' performance (Hardy et al., 1999; Cotter et al., 2003; Viet et al., 2017; Arnone et al., 2021). Testing the model output accuracy in relation to the input spatial resolution can give insights about the practical application of a proposed distributed model.

In this work, the first application of CRITERIA-3D for predicting landslides' occurrence in a seminatural environment is presented. CRITERIA-3D is a physically-based distributed model including an agro-hydrological module that solves soil-water balance accounting for transient vegetation activity and evolution, snow accumulation and melting, solar radiation and soil cracking formation. The original agro-hydrological module of CRITERIA-3D (Bittelli et al., 2010) has been extended introducing a slope stability computation module, based on the limit equilibrium theory within the infinite slope scheme framework. The model allows to obtain time-varying maps of the Factor of Safety (FoS), which is calculated at different depths, considering the presence of different soil layers and related parameters. The model is able to consider the differences existing in space and time of both canopies' development and root density. Based on the validation carried out only in one dimension (CRITERIA-1D, Sannino et al., 2024) the complete 3-dimensional model has been validated back-analyzing a real landslide occurred during the monitoring period on a test slope. Results showed that CRITERIA-3D is able to reproduce with high accuracy the field water content, the soil water potential behavior and the aerial geometry of the landslide. The effect of different spatial resolutions of the input Digital Elevation Model (DEM) has been tested in terms of both hydrological parameters and FoS of the slope. Some differences due to the DEM resolution have been observed on the FoS more than in hydrological parameters' computation.

2. Model description

The agro-hydrological CRITERIA-3D model (Bittelli et al., 2010), after being improved and extended to slope stability analyses in one-dimension (Sannino et al., 2024), has been adopted to carry out a three-dimensional slope stability analysis on a test slope. This section describes the basic components of the model, highlighting the further improvements developed in the present research. It is worth specifying that, in the following, the term "water potential" is used as equivalent to "soil suction".

2.1. Hydrology

The CRITERIA-3D model (Bittelli et al., 2010) is based on a numerical solution of the three-dimensional Richards' equation. The model solves a global soil-water balance equation, coupling surface and subsurface flows, computing soil water fluxes and embedding conceptual models for crop development, evapotranspiration, snow accumulation and melting, and solar radiation, based on hourly weather data (Fig. 1). The needed input data are: a Digital Elevation Model (DEM) of the area of interest; an hourly meteorological time series comprising air temperature, precipitation, solar radiation, wind intensity and relative humidity records; a soil map with the parametrization of the different soil layers; a land use/crop map with the related parameters.

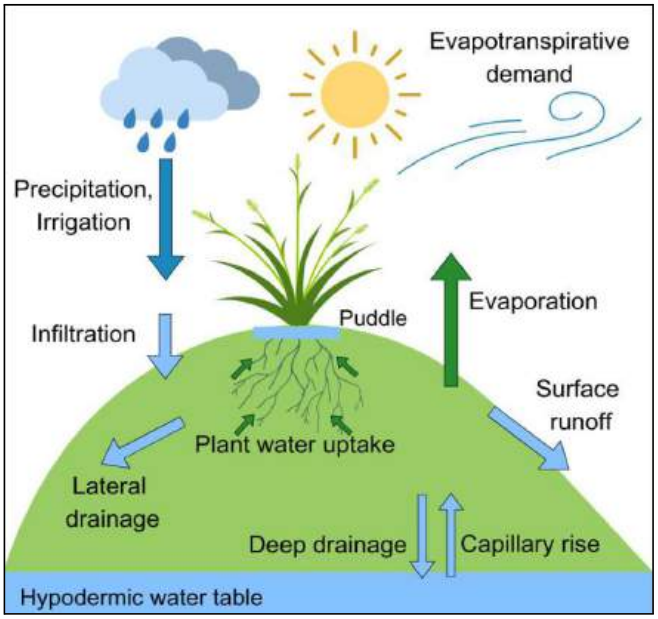

Fig. 1. Representation of the CRITERIA-3D soil-water balance.

CRITERIA-3D is able to consider multi-layered soil units, where each layer is characterized by different hydrological parameters and soil-water retention curves on the basis of the modified Van Genuchten-Mualem model proposed by Ippisch et al. (2006). This latter can be either texture-based or field-derived, in the sense that fitting values for specific water potential values can be provided.

The computation domain in CRITERIA-3D is discretized based on the Digital Elevation Model (DEM) used, which can be explored through a 3D interface. The DEM spatial resolution constitutes the 2D surface mesh. In plan, land use, soil and topographic maps are provided as Arcview Binary Raster format (.flt).

Along the soil depth, computational layers with different thicknesses are set according to a geometric progression, which considers the shallow layers to be divided more finely with respect to the bottom ones. In fact, over the shallow portion of the soil, effects of evaporation, solar radiation and canopy coverage produce more complex soil-water fluxes that can be better represented when the vertical discretization is thinner. Soil information such as layer parameters are provided as SQL databases (.db).

Results can be obtained in terms of maps (.flt) at specified hourly time steps for all the computational soil layers, and also in terms of hourly time series (.db) on selected output points. For both types of outcomes, the output variables can be referred to specific soil depths. Out of default results, the volumetric water content, the water potential and the degree of saturation can be required as model outcomes.

The infiltration in the first layer is governed by its water content and its hydraulic conductivity, and by the surface boundary conditions. A pond depth connected to the presence of vegetation can be set, in order to simulate the effect of water accumulation. The pond is useful to simulate a delay in runoff process initiation, due to the presence of vegetation, during a rainfall event. The runoff is also regulated by the roughness parameter, which depends on the kind of vegetation. Canopies are also involved in the soil-water balance through the reduction of evaporation. Subsurface water movements across adjacent nodes are governed by hydraulic conductivity gradients, and develop as redistribution movements in all directions after the water infiltrates into the soil (Bittelli et al., 2010).

Although the one-dimensional approximation of water movements is normally referred to the vertical infiltration, in some cases the hydraulic conductivity along other directions may be different and higher than the vertical one, due to the soil pore structure (Yuan-Shu et al., 2008). The

ratio between horizontal and vertical hydraulic conductivity, either saturated or unsaturated, is a measure of the hydraulic soil anisotropy, which depends on soil texture, on the current water potential, and on the variability range of hydraulic conductivity (Mualem, 1984). Although it is a complex phenomenon, for fine-textured soils some authors discussed how the unsaturated anisotropy ratio decreases toward a minimum value the more the soil dries (Assouline and Or, 2006). A slight increase, after the minimum value is reached, is then observed until the soil approaches the minimum degree of saturation.

In the CRITERIA-3D model it is possible to set a static horizontal/vertical hydraulic conductivity ratio, although it was shown that it is a temporally variable parameter (Petersen et al., 2008; Bagarello et al., 2009). The anisotropy ratio can help to increase the accuracy of the hydrological simulation in terms of numerical convergence. The required level of accuracy can be set by the user, on the basis of the desired model performance. Decreasing the required accuracy or using a wider DEM spatial resolution helps in the reduction of the computation time. The main output of the hydrology computation are the volumetric water content and the water potential for each soil layer.

2.2. Snow accumulation and melt

The snow melt is simulated in CRITERIA-3D based on the algorithm presented by Brooks (2003) and Brooks et al. (2007). The method is based on mass and energy balance computed for the snow pack. Snow accumulation in drifts is derived through the Snow Tran-3D model (Liston and Sturm, 1998), adjusted for the wind speed hourly measurements. The model, derived by Brooks (2003), was modified in CRITERIA-3D by Bittelli et al. (2010) introducing the effect of stream flow kinetic energy, the runoff liquid water temperature, the advective exchange between the runoff water and the snowpack. The snow accumulation and melting simulation allows the water infiltration to be delayed when the air temperature is at or below 0 °C. More details are provided in Bittelli et al. (2010).

2.3. Soil cracking

An improvement with respect to the original version of CRITERIA-3D (Bittelli et al., 2010) is represented by the implementation of a conceptual model for soil cracking formation. In fact, as the hydrology is governed by matrix flow equations such as Darcy's law, the model was originally designed for undeformable and uniform soils. In order to appropriately simulate the hydrological behavior of fine soils, especially when there is a high percentage of fine particles, conceptual models were considered as possible solutions. In the updated version of CRITERIA-3D, it is assumed that cracks start to form when the void fraction overcomes a user-selected threshold. The void fraction is identified as the difference between the saturated soil water content and the current soil water content. After this threshold, cracks continue to enlarge until the void fraction reaches a user-defined upper boundary, where the soil cracking is at its maximum development. At this point, the soil is considered occupied by soil desiccation cracks for a certain percentage, which is set equal to 5 % by default. Between the two boundaries, the soil cracking formation continues linearly (Cheng et al., 2020) (Fig. 2).

The soil percentage occupied by cracks is converted into an amount of infiltrating water that fills the soil layers from the bottom upwards. This water amount is calculated per each unit thickness of the soil (in centimeters), and starts from the maximum cracking depth, which is user defined. At this depth, a positive flux amount (mm/cm) is assigned. Depending on the rainfall amount falling, the crack will continue to be filled as long as voids and rainfall are present. This effect will occur only if the encountered soil layers, from the maximum cracking depth to the surface, have fine fraction content, defined as the sum of silt and clay content, higher than 50 %, and in relation to the gravel percentage. In fact, as shown by Yesiller et al. (2000), the percentage of fines in a soil is an important factor in causing desiccation cracking (Safari et al., 2014).

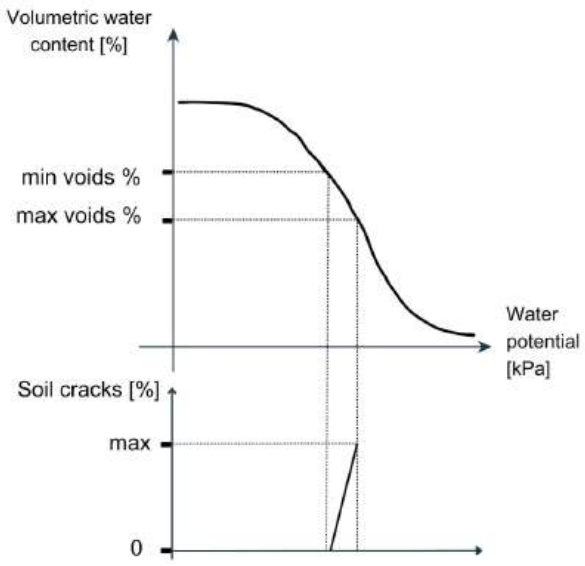

Fig. 2. Schematic representation of the CRITERIA-3D soil cracking conceptual model.

With this conceptual model, CRITERIA-3D approximates the first-order crack formation; in fact, these cracks are wider and longer compared to the second- and third-order cracks (Yuan-Shu et al., 2008). As only the soil permeability changes with the pore size distribution, maintaining the same SWCC (Li et al., 2011) and assigning a positive flux to nodes interested by the cracks' formation can be considered an appropriate assumption.

2.4. Crop modeling

The crop modeling approach is the same adopted in the CRITERIA-1D model, which is described in Sannino et al. (2024), and in the CRITERIA-1D/3D technical manuals (Antolini et al., 2016; Tomei et al., 2024). Growth and decay of both roots and canopies throughout the year are modeled based on real meteorological data through the growing thermal time of the crop (Ritchie and Nesmith, 1991; Trudgill et al., 2005). Depending on air temperatures, the vegetation stores specific amounts of heat based on a thermal threshold. These heat amounts are accumulated in *growing degree days* (GDD, Sannino et al., 2024). Specific thresholds are set in order to determine whether the plants accumulate heat and are in selected phenological stages. This scheme is adopted in CRITERIA-3D for both crops and natural environments, and the different growing phases can be modified to approximate the real phenology of the considered species, in a specific habitat. Moreover, CRITERIA-3D allows to consider different land uses, as input maps, in terms of vegetation type. Each vegetation type is characterized by specific parameters conceiving the plant species, the roots' architecture and depth, the evapotranspirative activity, the growing degree days that are necessary to change phenological stage, the canopy development over the year, and the crop coefficient kc (Guerra et al., 2016).

After the vegetation emergence, maximum evaporation and maximum transpiration are derived from the reference evapotranspiration (ET_0), following the approach of Driessen and Konijn (1992) with some modifications. The maximum evaporation (E_{max}) is defined through Eq. 1:

$$E_{max} = (1 - K_c)^{*} ET_0 \quad (1)$$

While the maximum transpiration (T_{max}) is derived through Eq. 2:

$$T_{max} = K_c^{*} TC^{*} ET_0 \quad (2)$$

Where $TC = 1 + (K_{cmax} - 1)*K_c$; TC is the turbulence coefficient [−], defined through the maximum value of K_c (K_{cmax}) as proposed by Doorenbos and Kassam (1979).

The crop coefficient k_c is a function of the leaf area index (LAI) (Eq. 3):

$$k_c = 1 - e^{-k_e LAI} \quad (3)$$

Where:
k_c = crop coefficient [−];
k_e = extinction factor, equal to 0.5 [−];
LAI = Leaf Area Index [−].

Reference evapotranspiration (ET_0) is obtained on an hourly basis through the Penman-Monteith method as reviewed by Allen et al. (1994). ET_0 depends on solar radiation, wind intensity, air temperature, and relative humidity (Eq. 2). Potential evaporation and transpiration are then limited to their actual values by the effective soil water availability

$$ET_0 = \frac{0.408\Delta(R_n - G) + \gamma \frac{900}{T_{avg}+273} u(e_s - e_a)}{\Delta + \gamma(1 + 0.34u)} \quad (4)$$

Where:
ET_0 = reference evapotranspiration [mm];
R_n = net solar radiation [MJ/m^{2}d];
G = net heat flow from the ground [MJ/m^{2}d];
Δ = slope of the function of saturated vapor [kPa/°C];
γ = psychrometric constant [kPa/°C];
T_{avg} = average air temperature [°C];
u = daily average wind speed at 2 m height [m/s];
$e_s = 0.6108e^{\frac{17.27Tavg}{Tavg+237.3}}$ is the average pressure of vapor in air saturation [kPa];
e_a = average pressure of vapor [kPa].

In these terms, the evapotranspiration is obtained on an hourly basis as a function of both meteorological data and vegetation condition, as the crop coefficient Kc is used to compute the actual hourly transpiration and evaporation from the reference evapotranspiration, passing through the maximum possible values. In fact, E_{max} and T_{max} (Eq. 1 and 2) are then reduced to the actual values based on the real soil moisture condition of the shallow layers and the rooted soil layers, respectively.

As already stated in the previous "hydrology" section, in CRITERIA-3D a pond depth can be set. This depth is used to assess the amount of water that is necessary to be accumulated before runoff starts and to compute the actual evaporation as well. It is a proxy for how much canopies can decelerate the rainfall infiltration. The maximum pond depth is reduced as a function of the actual leaf area index (that depends on the phenological stage of the plant) and the local slope, in order to approximate the effect of real morphology on the interception action of canopies.

2.5. Boundary conditions

The following default boundary conditions are set in CRITERIA-3D: free runoff at the surface nodes and free drainage at the bottom layer nodes. Atmospheric boundary conditions can be either positive flux (precipitation) assigned to the surface, or negative flux (potential evapotranspiration) assigned to the layers where roots are present. From a temporal point of view, CRITERIA-3D uses meteorological input data corresponding to at least one year to set up an accurate initial wetness state of the soil domain.

2.6. Slope stability

The slope stability is assessed through the calculation of the Factor of Safety (FoS) for each computational element. The computational elements are constituted by rigid soil cells, with a cross section area corresponding to the DEM spatial resolution and a thickness corresponding to that of each soil layer (Fig. 3). This allows the CRITERIA-3D model to calculate FoS at different depths.

The limit equilibrium method within the infinite slope framework is adopted (Sannino et al., 2024). The soil is assumed as a rigid-plastic material and its shear strength is expressed through the Mohr-Coulomb criterion.

The equation used to calculate hourly values of FoS is derived from Lu and Godt (2008) (Eq. 5). Based on the suction stress (σ^s) concept, the method takes into account the whole range of soil moisture conditions and their effect on soil strength:

$$FoS = \frac{tan\varphi'}{tan\beta} + \frac{2c_{tot}}{\gamma H_{ss} sin2\beta} - \frac{\sigma^s}{\gamma H_{ss}}(tan\beta + cot\beta)tan\phi' \quad (5)$$

Where:
$\sigma_s = -\frac{\theta - \theta_r}{\theta_s - \theta_r}(u_a - u_w)$;
$c_{tot} = c' + c_r$;
c' is the effective soil cohesion [kPa];
c_r is the root mechanical contribution [kPa];
θ is the actual soil water content [m^3/m^3];
θ_r is the residual water content at the wilting point [m^3/m^3];
θ_s is the saturated water content [m^3/m^3];
φ is the friction angle [°];
β is the slope angle [°];
H_{ss} is the depth of interest [m];
γ is the unit weight of the soil [kN/m^3].

The different soil layers can be characterized by different parameters. The time-varying suction stress is determined based on the hydrological outputs (volumetric water content and soil-water potential). The soil strength parameters are: the effective cohesion (c'), the friction angle φ'. The bulk density is converted to soil unit weight (γ). These parameters can be user-defined, otherwise CRITERIA-3D can assign them based on the soil texture, using empirical pedotransfer functions. Specifically, parameters' values were derived from García-Gaines and Frankenstein (2015), based on soil classes from the Unified Soil Classification System (USCS, Casagrande, 1948) associated with those from

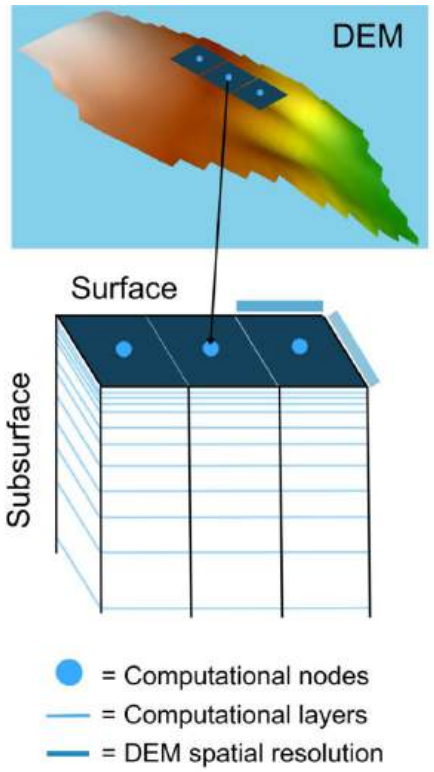

Fig. 3. Schematic representation of the CRITERIA-3D computation domain.

the United States Department of Agriculture (USDA, Kellogg, 1937; Ditzler et al., 2017). The texture-derived values of these parameters are considered to be highly approximative and their use is recommended only if there is lack of experimental data or no available data in literature. The root cohesion (c_r) must be selected by the user. If the maximum root cohesion is available as derived by literature studies or field measurements, it could be inserted as a crop parameter and it will be associated to the soil layer with the maximum root density. Then, the value will be reduced based on the real presence of roots in the other soil layers.

3. Test slope at Montuè

The CRITERIA-3D model has been validated based on field data acquired on a test slope, which is located in Montuè, Northern Apennines, Italy (Fig. 4). A monitoring station has collected meteorological and soil data since 2012 (Bordoni et al., 2015, 2021). A sketch of the monitoring station and the installed sensors is provided in Fig. 5. The integrated monitoring station includes a rain-gauge, a thermo-hygrometer, an anemometer, a net radiometer, and a barometer, as meteorological sensors. Moreover, six time-domain reflectometer probes with a multiplexer are installed at 20, 40, 60, 100, 120, and 140 cm to measure soil water content, while three tensiometers and three heat dissipation sensors are installed at 20, 60, and 120 cm from the ground level to measure the pore water pressure. Specific information about the installed sensors are provided by Bordoni et al. (2015) and by Sannino et al. (2024).

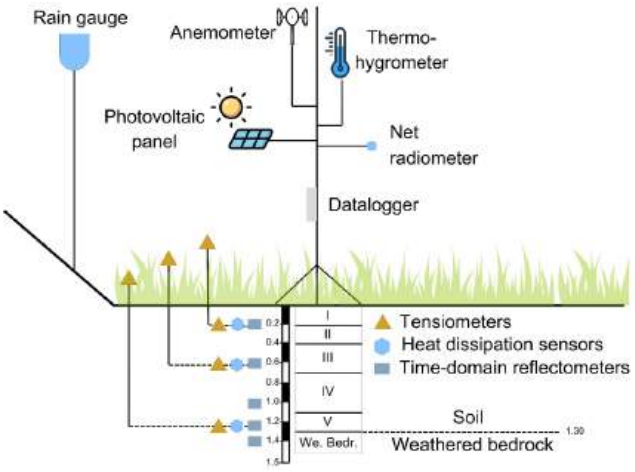

Fig. 5. The monitoring station.

The first documented shallow landslides in the area surrounding the test slope occurred in 2009, due to a rainfall of 160 mm in 62 h (Bordoni et al., 2015). After that event, the monitoring station was installed. A

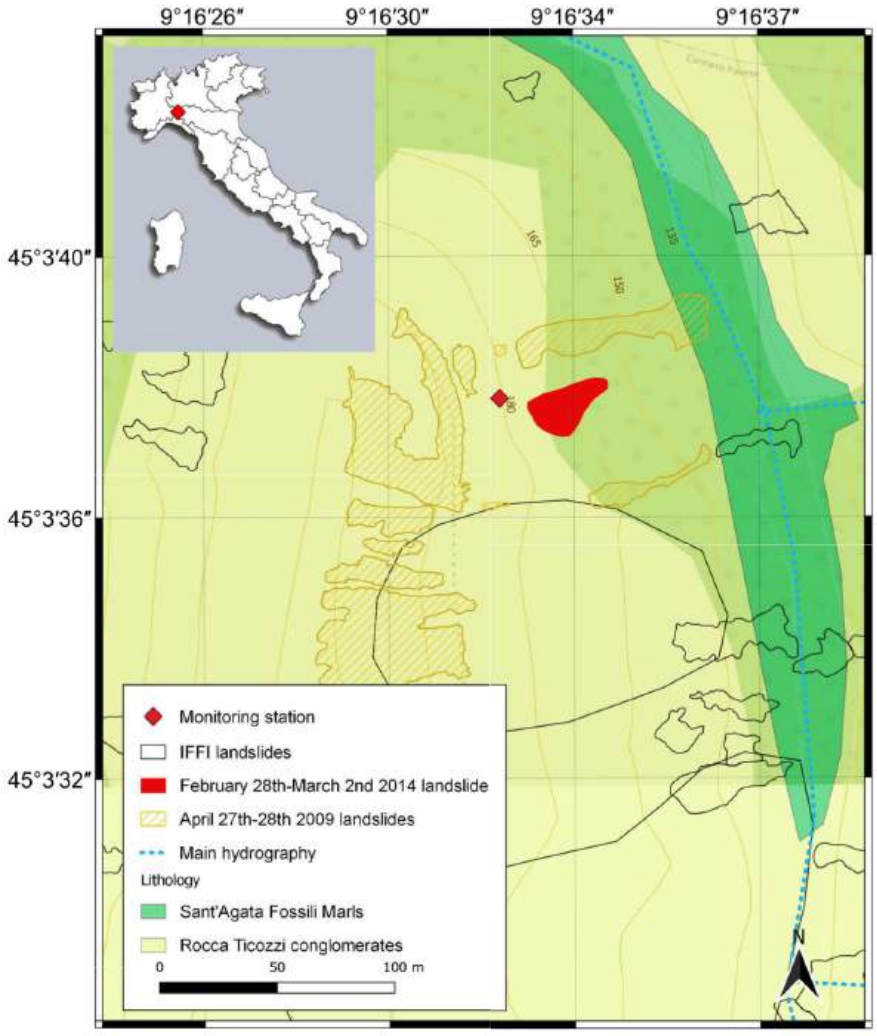

Fig. 4. Study area.

new shallow landslide occurred on the test slope, a few meters away from the monitoring station, between 28 February and 2 March 2014, at a depth of 100 cm, due to a rainfall event of 68.9 mm in 42 h (Bordoni et al., 2015).

4. Model application

4.1. Soil layers' parametrization

In this section, the parameters used to apply CRITERIA-3D in the case study of Montuè are described in detail. The soil layers are the same used in the CRITERIA-1D model simulation (Sannino et al., 2024) since the test site was the same. The values assumed for both mechanical and hydrological parameters, based on field experimental campaigns, are listed in Table 1 and Table 2, respectively. In particular, to compute the water potential and the equivalent degree of saturation, CRITERIA-3D uses the modified van Genuchten–Mualem formulation proposed by Ippisch et al. (2006). The hydraulic conductivity function is calculated through the approach presented by Mualem (1976). The parameters needed for the soil-water retention curves are: the curve fitting parameters α, n, m, and the air entry value h_e, which characterizes the transition between saturated and unsaturated regime. These parameters are estimated based on the soil texture and the fitting values, when provided. It is assumed that the soil layers are the same, keeping their constant thickness, everywhere along the slope.

As already discussed, in CRITERIA-3D soil hydrological anisotropy is simulated through the ratio between the horizontal hydraulic conductivity and the vertical hydraulic conductivity. In simulations related to the Montuè test site this ratio has been set equal to 4. This ratio is applied both at unsaturated and saturated hydraulic conductivities, and, due to the lack of more accurate data, it was calibrated according to field water content data and simulation outputs.

The considered simulation period spans from 1st January 2012 to 30th April 2014. In this way, a period of at least one year before the landslide occurrence could be simulated, in order to reproduce a reliable soil moisture condition at the date of the landslide. Indeed, the landslide was triggered at an unspecified time during the rainfall event that occurred between 28th February and 2nd March 2014. By observing the field data, it was evident that the soil at Montuè underwent the formation of desiccation cracks during the previous dry season (summer) in 2013, evidenced by an uprising of soil water content at 40 and 60 cm of depth without a corresponding increase of water content in the upper and lower layers (Sannino et al., 2024). The parameters chosen to simulate the soil cracking formation, based on field water content and pore water pressure records, are listed in Table 3.

The upper and lower bounds of void percentage were chosen in order to represent a range of moisture below the field capacity water content (i.e., the soil water content when all the micropores are filled) and higher than the wilting point water content (i.e., when the residual water is immobilized by the soil particles). This simplification, in absence of more detailed data, was adopted also according to the field observations (Bordoni et al., 2021). Some authors highlighted that crack develops until a steady-state development stage, and the crack opening, intended as the soil volume occupied by cracks, varies from 0 to approximately 5 % (Li and Zhang, 2011). The value of 5 % as maximum soil percentage covered by cracks was selected also according to literature data for vegetated soils and soils reinforced with vegetation fibers (e.g. Safari et al., 2014; Trabelsi et al., 2018: Wardhana et al., 2021). The soil crack percentage is converted in a positive flux of 0.5 mm/day assigned firstly to nodes at 60 cm of depth and to the above nodes up to the surface, only if the fine fraction, defined as the percentage of total clay and silt content related to the coarse fragments content, is more than 50 %; this threshold was chosen to represent the fact that the soil crackings only form when the soil is fine-textured enough, even if the voids percentage is between 15 % and 20 %. Since at the Montuè test site this threshold is overpassed (Table 1), soil cracks are considered to have formed up to 60 cm of depth.

4.2. Land use and vegetation parametrization

The land use at the test site was derived from aerial photographs of 2009 (when other landslides occurred) and 2014, assuming that the 2009 coverage was valid for the whole simulation period, in absence of more detailed data. By observing the satellite photographs, three land uses were detected: a bare soil corresponding to a trail, a shrubland, and a young woodland. The 2014 landslide occurred in the woodland zone, just behind the transition between the two land uses (Fig. 6a). It is evident that some vegetation has grown around the monitoring station after 2009.

Fig. 6b reports the landslide scar, the monitoring station, and the output points chosen to validate the model outputs. More precisely, a point was chosen to represent the monitoring station (MS) and the other 5 points represent the landslide (points L1, L2, L3, L4 and L5).

The 1-m DEM is considered to appropriately represent the real topography of the test slope, as it is the most accurate available. It was realized through LiDAR data acquired in 2008 and 2010 by the Italian Ministry for Environment, Land, and Sea, and it represents a reliable pre-event topography condition as it is the closest in time. The planimetric accuracy is 30 cm, and the altimetric accuracy is 15 cm.

The selected computational area has an extension of 14,547 m^2 and has been subdivided according to the real land uses. As it will be explained in the following, this starting DEM has been resampled, in order to test the sensitivity of the simulation in relation to different DEM spatial resolutions. The different types of vegetation and land use present were parameterized through the values listed in Table 4. Fig. 7 reports a comparison between the difference in LAI development, evaporation and transpiration activities over the 2014, i.e. the year when the landslide occurred, for the two chosen land uses.

4.3. Model settings

In order to test the model performance, different analyses have been carried out by changing the DEM spatial resolution. The starting DEM with a resolution of 1 m was resampled through the algorithm *saga: resampling* by QGIS, deriving DEMs with spatial resolutions of 2 m, 5 m, and 10 m. The analyses were conducted keeping constant values of all other input parameters (i.e., the meteorological records, soil and crop parameters) and the same output control points. The aim was to test whether the CRITERIA-3D model is sensitive to different input resolutions. As represented in Fig. 6b, six output control points were selected:

Table 1
CRITERIA-3D mechanical parameters at Montuè test site for different soil layers.

Soil layer	Depth range [cm]	Coarse fragment [%]	Organic matter [%]	Sand [%]	Silt [%]	Clay [%]	Bulk density [g/cm^3]	c' [kPa]	ϕ' [°]
I	0–22	0	1.44	16.6	58	25.4	1.559	0	31
II	22–42	0	1.36	11.9	59.9	28.2	1.534	0	31
III	42–70	0	1.03	16.0	53.9	30.1	1.495	0	33
IV	70–110	0	0.88	12.6	57.9	29.5	1.518	0	33
V	110–130	0	0.62	7.7	65.8	26.5	1.418	29	26
We. Bedr.	130–145	0	0.2	75	25	0	1.532	29	26

Table 2
CRITERIA-3D hydrological parameters at Montuè test site for different soil layers.

Soil layer	Depth range [cm]	Θ_r [m^3/m^3]	Θ_s [m^3/m^3]	K_{sat} [m/s]	h_e [kPa]	α [kPa-1]	n [−]	m [−]
I	0–22	0.00	0.40	7E-07	2.6	0.049	1.279	0.218
II	22–42	0.01	0.41	2E-07	3.1	0.049	1.290	0.225
III	42–70	0.00	0.43	2E-07	3.1	0.044	1.243	0.195
IV	70–110	0.00	0.42	3E-07	3.1	0.104	1.310	0.237
V	110–130	0.04	0.46	3E-07	2.6	0.049	1.263	0.208
We. Bedr.	130–145	0.01	0.42	2E-07	1.0	0.034	1.329	0.247

Table 3
Soil cracking parameters.

Maximum soil crack depth	60 cm
Minimum voids for cracks formation initiation	15 %
Voids for cracks formation ending	20 %
Maximum soil percentage covered by cracks	5 %

Fig. 6. Land use (a) and location of the monitoring station, landslide and output points (b) at Montuè case study.

Table 4
Soil land use and crop parameters at Montuè test site.

Land use	Shrubland		Woodland		Road
LAI [m^2/m^2]	min	0.5	min	1.0	–
	max	3.0	max	4.0	
Root depth (RD) [cm]	RD_0	0.05	RD_0	0.05	–
	RD_{max}	1.4	RD_{max}	1.45	
Thermal thresholds [°C]	lower	3	lower	0	–
	upper	35	upper	35	
Degree days [°C]	phase 1	1000	phase 1	2500	–
	phase 2	1000	phase 2	1000	
k_c max [−]	1		1		–
LAI curve factors [−]	a	4.1	a	4.1	–
	b	−0.014	b	−0.014	
Root architecture shape	cardioid		cardioid		–
Root shape deformation factor [−]	0.0		0.0		–
Ψ_{leaf} [kPa]	1470.96		1569.02		–
C_r [kPa]	–		–		–
Roughness [$s/m^{1/3}$]	0.05		0.1		0.03
Pond depth [m]	0.006		0.006		0.003

one represents the position of the monitoring station (point 'MS'), which has been used to validate both water content and water potential simulations; four out of other five points are positioned along the scar contour and one point is in the middle of the 2014 landslide (points named 'L' followed by numbers). Hourly results related to the vertical positions where sensors are installed (namely, at 20, 40, 60, 100, 120, and 140 cm of depth) have been analyzed individually and also averaged, in order to obtain mean values related to the whole soil profile. Field hourly data related to the same depths have been also averaged for comparison. Hourly slope stability analyses were conducted using the different DEMs, and FoS was calculated at selected computational depths (namely, at 1, 3, 5, 10, 20, 60, 100 and 120 cm); however, only the hourly outputs related to representative depths of 10, 60 and 100 cm will be presented in the following section.

5. Results and discussion

5.1. Hydrological results

As already stated, different depths were selected for the hydrological computation and results were averaged. For the sake of conciseness, Fig. 8 shows the comparison between the mean values of both observed and computed soil water content. Fig. 9 shows the comparison between the values of observed and computed water potential at 60 cm of depth, which is the depth with less missing values in the field measurement series. The R^2 values reported in Table 5 and in Table 6 are related to the comparison between modeled and observed values of the volumetric water content (VWC) and the water potential (WP), respectively, at the investigated depths for different DEM resolutions. Specifically, the values correspond to the output point called 'MS' (Fig. 6b).

The different DEM spatial resolutions considered seem not to have a significant impact on the soil water content and soil water potential

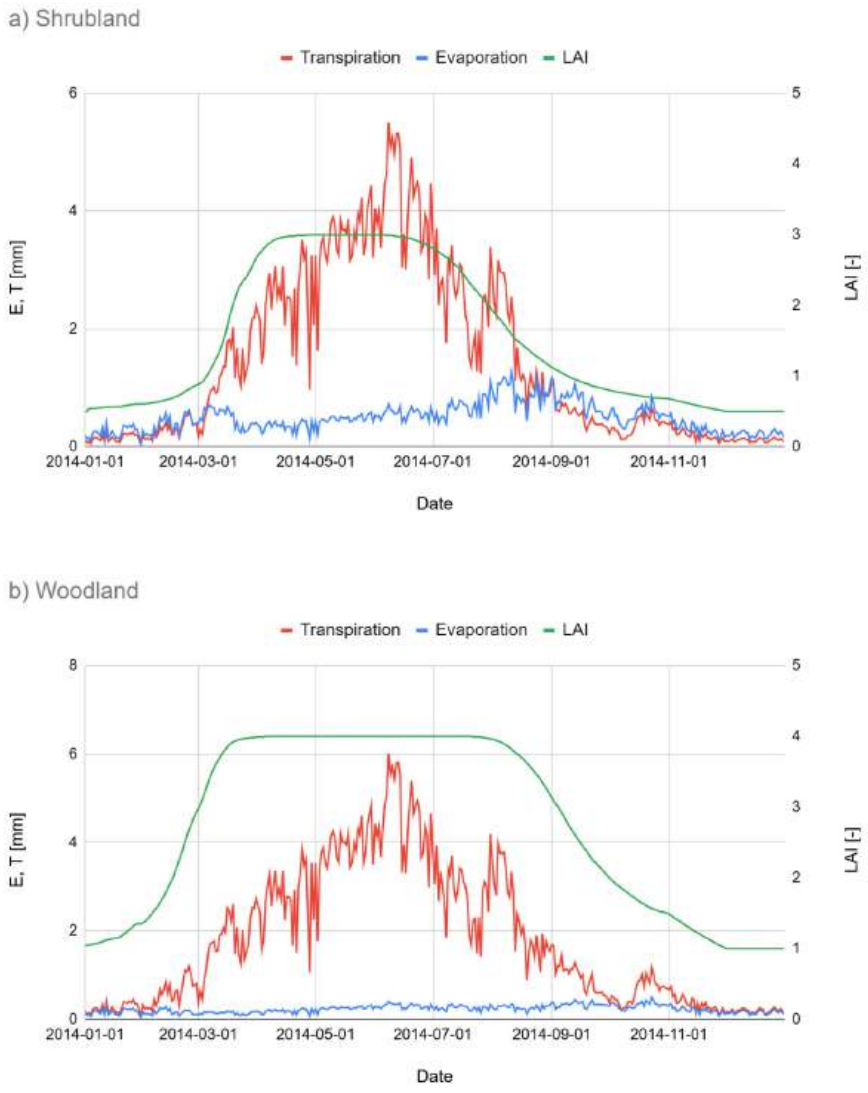

Fig. 7. Leaf Area Index (LAI, green line), transpiration (T, red line), evaporation (E, blue line) development over the landslide year 2014 of both the land uses: shrubland (a) and woodland (b). (For interpretation of the references to colour in this figure legend, the reader is referred to the web version of this article.)

simulations. This is maybe due to the limited spatial extent of the whole computational domain. The simulation conceiving the soil water potential obtained through a coarser DEM resolution has the best performance at all the considered depths (Table 6). For what concerns the soil water content, results' accuracy changes depending on the considered depth, and it is not possible to declare which DEM provided the best results. If the whole averaged soil water content is considered, the 5 m-DEM seems to provide the most accurate simulation, although only little differences are present among the different simulations.

Fig. 10 and Fig. 11 report the model results in terms of time-varying hydrological maps related to the test slope. In particular, Fig. 10 reports the output in terms of volumetric water content, and Fig. 11 reports the output in terms of water potential. The maps refer to two different time instants, which are representative of the states before and after the landslide occurrence, respectively. The first selected time is at 6 a.m. on 1 March 2014, i.e. one day before the triggering of the landslide, as detected by CRITERIA-3D; the second selected time is at 6 a.m. on 2 March 2014, i.e. when the instability reaches 100 cm of depth, based on the model simulation, as it will be explained in the following section on FoS. The maps, which have been derived using the 1 m-DEM for computation, report the results corresponding to the representative depths of 30, 60, 100, and 140 cm, even though similar results are available for all the different computational depths.

As shown in Figs. 10 and 11, for what concerns the hydrological conditions during the landslide occurrence, the maps related to the most superficial layers appear to be more homogeneous than those related to higher depths. In fact, soil water accumulates more in the hollow portions of the slope, which can be easily recognized in the maps as the slope area beneath the landslide scar and the area located some meters away from it. At the border of the computational domain, some pixels are also computed as saturated (nil or positive values of WP, Fig. 11) and a slight concave area is also present there. The effects on hydrology exerted by the surface topography appear to be well captured by the three-dimensional model.

By looking at the hydrological output maps, it could be assumed that the landslide has occurred because of the saturation of the soil profile down to 100 cm of depth. The water seeping downward and the lateral subsurface processes provoke the saturation of the hollows, and the shallower layers seem to saturate earlier in time, as they have a high moisture level while the underlying layers still don't (Fig. 10). More precisely, the infiltration process seems to be slowed down in the soil layer III (Table 1, 2 and Fig. 5), which develops between 42 and 70 cm of

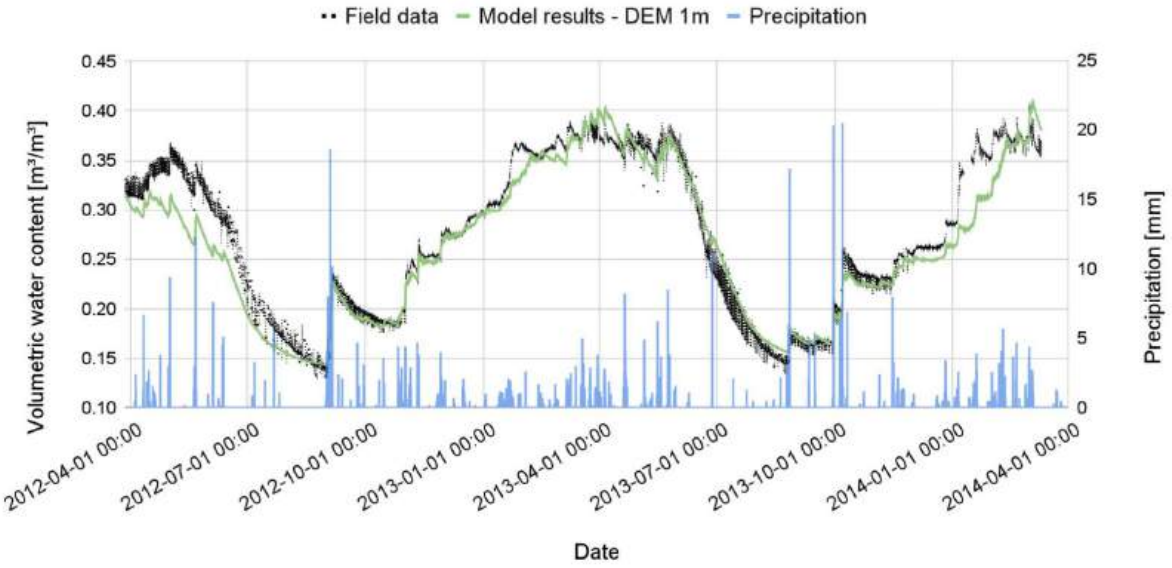

Fig. 8. Comparison between mean values of simulated and observed water content for the whole soil profile (0–145 cm) using the 1 m-DEM.

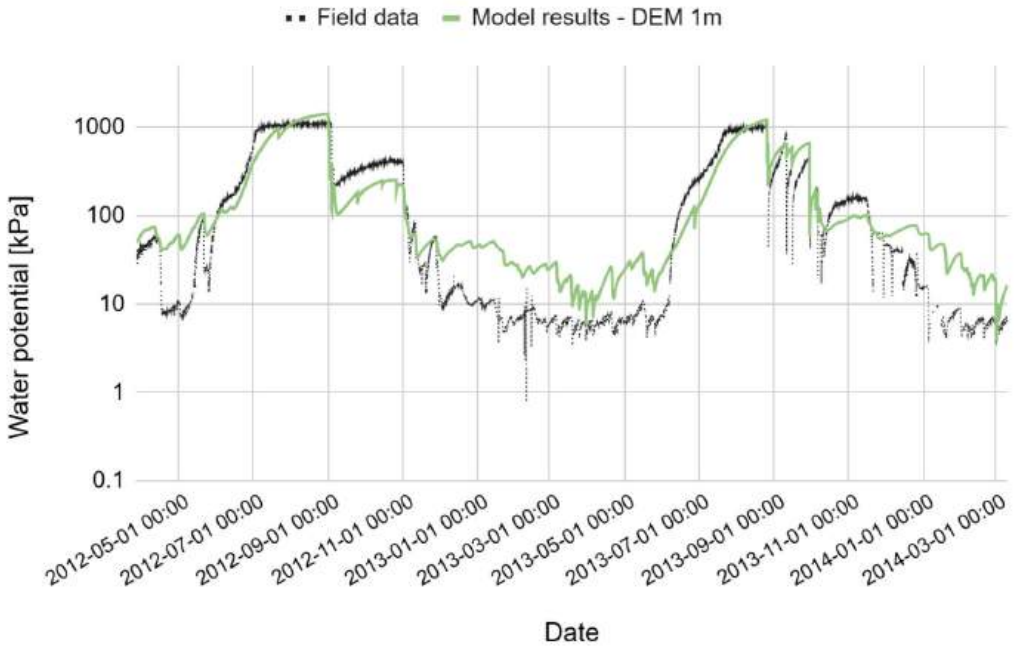

Fig. 9. Comparison between simulated and observed water potential at depth of 60 cm using the 1 m-DEM.

Table 5
Comparison between modeled and observed values of volumetric water content (VWC), at different depths and with different DEMs, in terms of R^2 at the output point 'MS'.

DEM resolution	20 cm of depth	40 cm of depth	60 cm of depth	100 cm of depth	120 cm of depth	140 cm of depth	Whole profile 0–145 cm
1 m	0.911	0.915	0.898	0.918	0.839	0.918	0.941
2 m	0.918	0.921	0.900	0.918	0.839	0.915	0.944
5 m	0.916	0.920	0.901	0.919	0.838	0.915	0.945
10 m	0.917	0.919	0.899	0.917	0.839	0.915	0.943

Table 6
Comparison between modeled and observed values of water potential (WP), at different depths and with different DEMs, in terms of R^2 at point 'MS'.

DEM resolution	R^2 observed vs simulated soil water potential at 20 cm	R^2 observed vs simulated soil water potential at 60 cm	R^2 observed vs simulated soil water potential at 120 cm
1 m	0.691	0.880	0.803
2 m	0.705	0.885	0.810
5 m	0.700	0.882	0.806
10 m	0.707	0.887	0.811

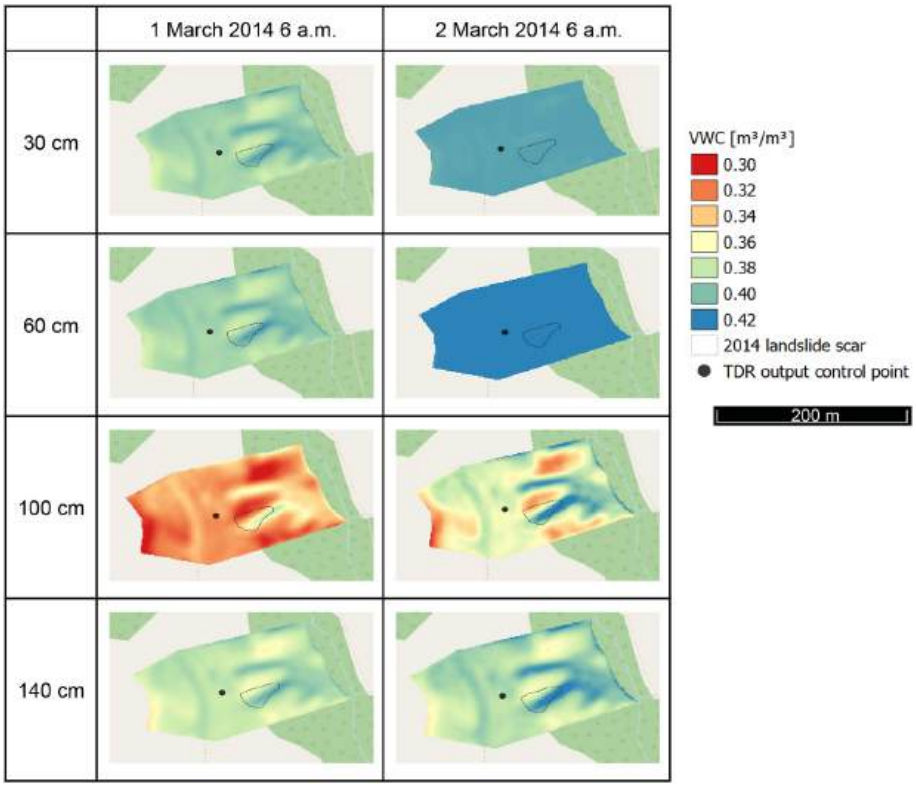

Fig. 10. Volumetric water content output maps before (1 March 2014) and during the landslide occurrence (2 March 2014) at different depths.

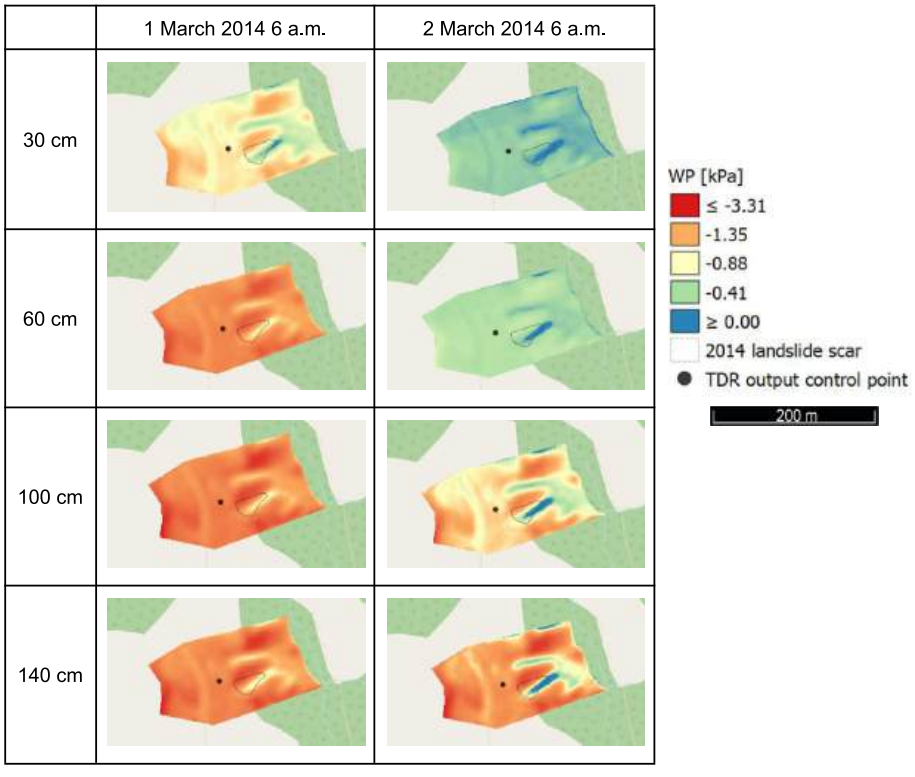

Fig. 11. Water potential output maps before (1 March 2014) and during the landslide occurrence (2 March 2014) at different depths.

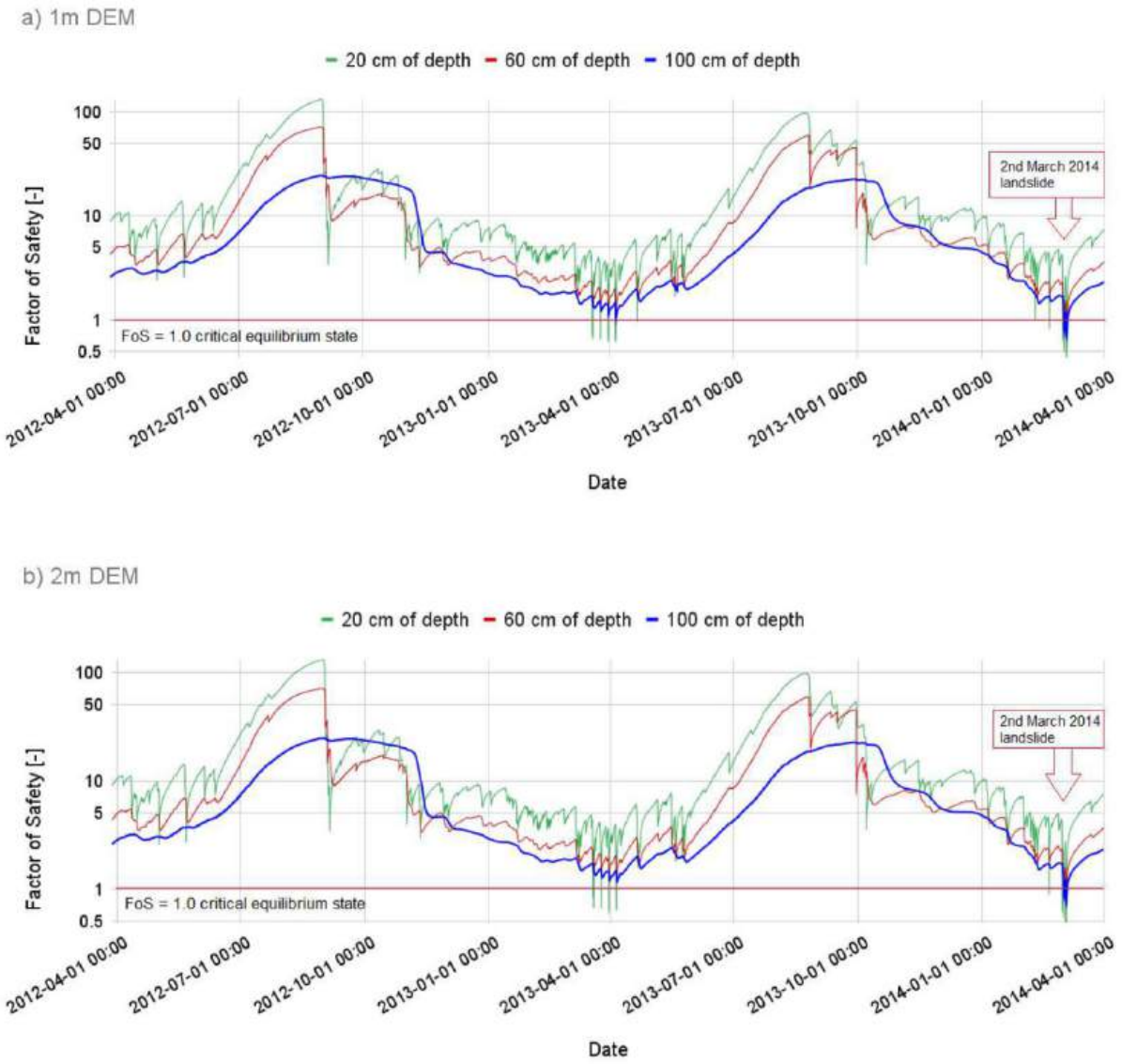

Fig. 12. Hourly Factor of Safety for different DEM spatial resolutions: a) 1 m b) 2 m c) 5 m d) 10 m. The dates are in format YYYY-MM-DD hh:mm.

depth. The depth of 60 cm belongs to this layer, and it is slightly more wet than the layer at 40 cm.

5.2. Slope stability analysis

Fig. 12 shows the trend of the Factor of Safety (FoS) in the analyzed time span, calculated at three different depths, i.e. at 20, 60, and 100 cm, respectively, assuming different DEM resolutions. It can be noticed that the unstable condition (FoS < 1) at 100 cm of depth, which is represented by the blue line in the graphs, is detected at a spatial resolution of 1 m, 2 m, and 5 m on the expected date of 2 March 2014. Indeed, 100 cm was the field observed depth of the failure surface (Sannino et al., 2024). Instead, when using the 10 m resolution DEM, the landslide is not detected by the model, as the FoS at 100 cm of depth never drops below one. On the other hand, FoS at 20 cm of depth (green line in Fig. 12) becomes lower than one several times, evidencing a sensitivity of the shallow soil layer to different rainfall events occurring during the wet season after winter, when the soil is nearly saturated.

Fig. 13 reports the resulting maps for the Factor of Safety obtained through the computational domain derived from different DEM resolutions. The maps refer to two different dates: 1 March 2014 at 6 a.m., i.e. one day before the landslide modeled occurrence, and 2 March 2014 at 6 a.m., i.e. when the unstable condition (FoS < 1) is reached at 100 cm of depth, which is the field observed depth of the failure surface.

As it could be observed from Fig. 13, the landslide is appropriately detected when adopting a DEM spatial resolution of 1, 2, and 5 m. Instead, using the DEM resolution of 10 m appears not satisfactory. This may be due to the attenuated effect of slope angles due to the topography simplification when reducing the DEM spatial resolution. Moreover, enlarging the DEM input resolution modifies the local detail of the input hydrological parameters, and so the instability conditions that may develop in a point of the domain could not be well represented, although the model responses to mesh variations can be complex and scale-dependent (Hardy et al., 1999; Schoorl et al., 2000; Tarolli and Dalla Fontana, 2009).

In all the simulations, except for the one with the 10 m DEM, at the border of the spatial domain some pixels are wrongly detected as unstable. This is due to the presence of a small depression, where infiltrated water accumulates. The topography effect is clearly visible in all the simulations, as the Factor of Safety (and thus, the water content)

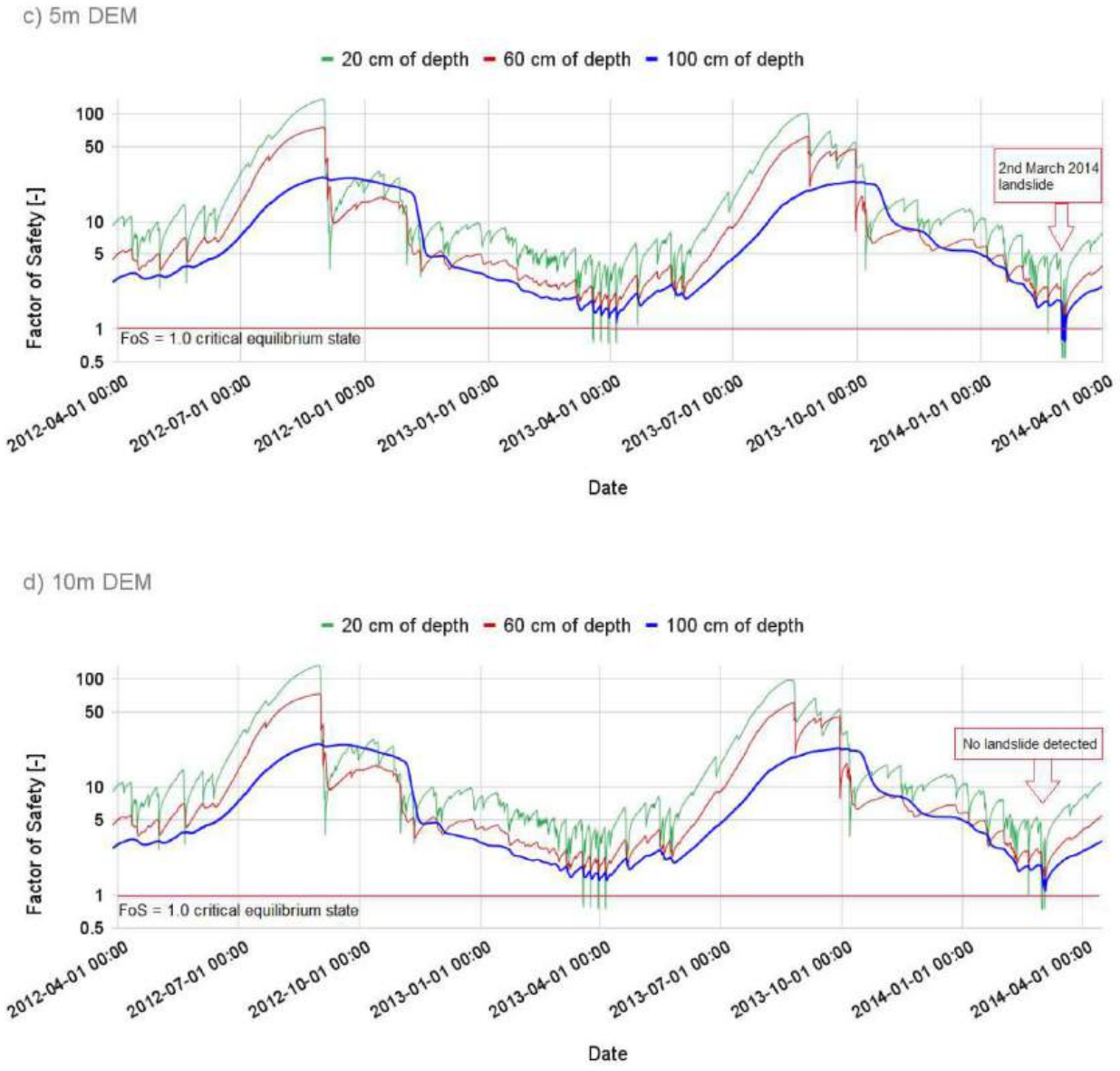

Fig. 12. (*continued*).

simulation clearly highlights the differences in hollow and caves present over the test slope.

It could be argued that the unstable pixels (the red ones in Fig. 13) only partially overlap the landslide scar. It can be observed that the proposed model adopts a simplified stability analysis where mechanical aspects such as the propagation of the instability due to deformations and movement of unstable portions of soils are neglected. Nonetheless, the results appear satisfactory in that the landslide-related hazard is appropriately assessed in both space and time.

Fig. 14 reports the model outcomes in terms of time-varying maps of Factor of Safety (FoS) calculated at different depths. FoS maps are shown referring to: a) different time steps, before and during the landslide occurrence, namely, 28 February 2014 (11 p.m.), 1 March 2014 (6 a.m.), and 2 March 2014 (6 a.m.); b) different depths, namely, 10, 30, 60, 100, and 140 cm of depth; c) 1-m spatial resolution DEM only. It can be seen that the landslide (FoS $<$ 1) is correctly predicted in the expected position, involving soil layers down to 100 cm of depth.

One day before the landslide, some pixels at 30 cm of depth are detected as unstable in the landslide body and at the border of the domain. Field data to corroborate whether some surficial processes like this have effectively occurred are not available. However, at the current model development, considering the lack of detailed data, obtaining very shallow soil portions detected as unstable is not considered as relevant for the shallow landslide prediction.

As it can be observed in Fig. 14, during the landslide (2 March 2014 at 6 a.m.), not only the landslide scar but other shallow portions of the domain are detected as unstable at 30 cm of depth, especially at the border of the computational domain and where a second hollow is present. The right border of the domain also corresponds to the lowest portion of the slope. Further studies will analyze in detail these outcomes in order to relate them to other processes such as erosion and to detect if such results can provide further information for land management purposes.

6. Discussion

Although the validation of the CRITERIA-3D model could be considered satisfactory, some model limitations are worth highlighting

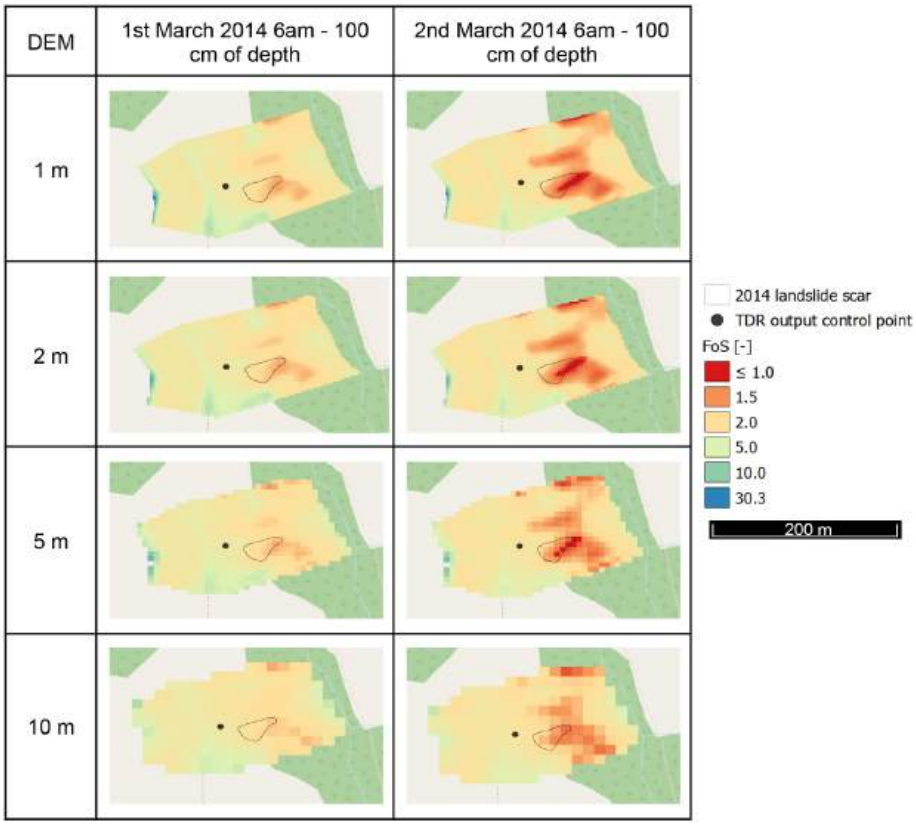

Fig. 13. Factor of Safety maps at 100 cm of depth for the different spatial resolutions before and after the 2014 landslide.

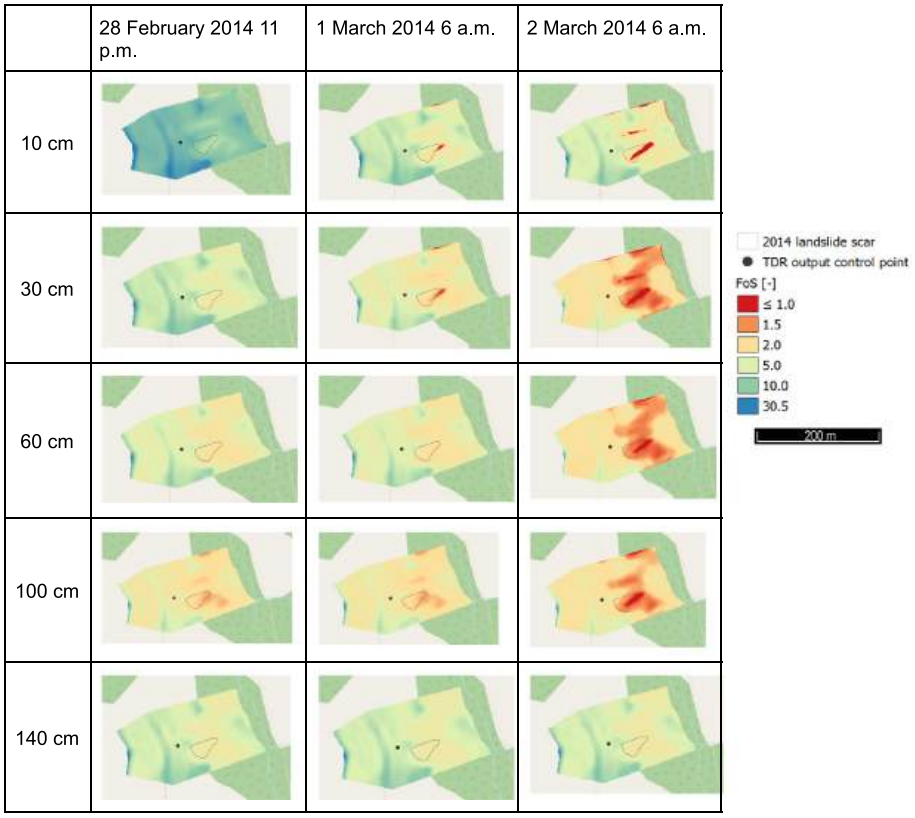

Fig. 14. Factor of Safety maps at different depths with 1 m-DEM before and after the 2014 landslide.

to ease the model application at other case studies. As regards the landslide prediction accuracy in terms of position, some differences have been observed by comparing FoS maps and FoS time series at specific control points. If on the one hand FoS maps appear rather satisfactory, the FoS computation at the output control points returned values below one - thus indicating instability - only in the lowest point of the real landslide scar ('L1' output point in Fig. 6) in a selected time. Such an outcome could be expected. The CRITERIA-3D model does not comprise bonds between adjacent cells, and when an elementary cell fails, the surrounding ones can keep the equilibrium until suction-induced reinforcement is lost. Moreover, as the subsurface hydrological processes are driven by water potential gradients, points at lower altitudes in the domain are those through which the water moves, inducing the corresponding soil cells to become more close to instability. Such an outcome must be kept in mind when applying the CRITERIA-3D model in other real case studies, especially where the topography is highly complex, defining multiple slope stability output control points. Instead, observing FoS maps, it must be kept in mind that, probably, not the whole landslide body will be detected as unstable at the same time. Depending on the topography and the DEM resolution, the number of cells with FoS lower than 1 can differ, and those with the highest slope will be the most likely to fail first.

Moreover, it is worth highlighting that when applying the CRITERIA-3D model to other case studies, any DEM can be used. The model is open-source, so that it can be used by any user. When choosing the spatial resolution of the DEM, which in turn affects the computational resolution, a compromise must be made between the quality of results and the speediness of the computation. This latter is clearly linked to the extension of the area of interest. Nonetheless, the choice of a certain DEM resolution depends on the orographic complexity of the area of application. However, limited to results of this case study, it seems that the optimal resolution is between 5 m (since at this resolution the landslide was still detected) and 10 m (as the landslide at Montuè was not detected anymore at this resolution). For what concerns soil layers' characterization, parameters can be manually set by users if field measurements or literature derived data are available. Based on the soil texture, CRITERIA-3D can estimate some parameters, such as the water content at saturation, the Van Genuchten-Mualem soil water retention curve parameters, the hydraulic conductivity, but a sensitivity analysis with regard to the model outcome is strongly recommended, as the parameters can be manually recalibrated. Moreover, it must be clear that estimated parameters are not always consistent with reality, as they can bring with them a big source of uncertainty. Soil mechanical parameters can also be estimated by the CRITERIA-3D model based on the work of García-Gaines and Frankestein (2015), although, as already discussed, these values must be used with caution. Vegetation parameters are instead provided in CRITERIA-3D for a set of reference crops and for woodlands and fallows. Any user can choose the annual development which is more suitable to the specific simulated case, or can create a specific one. Further detailed aspects, including instructions on how to prepare a proper meteorological input file, are better specified in the model manuals (Antolini et al., 2016; Tomei et al., 2024), which are available together with the open-source code. Thanks to the open-source and an intuitive interface, the model is easily accessible to both researchers and practitioners.

Future developments will include the code parallelization, in order to make the model faster when applied to larger areas maintaining a high resolution. Moreover, the possibility of adding a vegetation density map will be addressed, as it would allow differentiating areas, inside the same land use domain, based on the real presence of vegetation. In fact, vegetation effects - and more particularly, the root density distribution - could be another factor discriminating among the different spatial resolutions to be adopted. By adding a density map, the vegetation-related effect on soil hydrology will be either reduced or increased based on the effective presence of plants, and their differentiated effect on the slope stability could be analyzed more in detail. The vegetation density map, which will be defined through the contemporary use of variables such as the LAI and the crop coefficient k_c, could be prepared in a GIS environment through the digitalization of aerial photographs related to the period of interest, defining areas of the domain where maximum vegetation coverage is present and areas with a reduced presence of it. In this way, it is expected that the effects of vegetation could be more realistic, considering reduced or increased influence up to a maximum, where the soil coverage is total. The map could be provided as an input of the same type of other maps, which are actually needed to compute a case study in CRITERIA-3D (i.e., a .flt file).

Another interesting improvement could be the inclusion of soil depth maps, i.e. the implementation of an algorithm able to redistribute the soil layers' thickness based on the topography and real soil depth. In fact, it is known that the soil depth distribution depends on the topography, allowing deeper soil to be present in areas where the slope is less pronounced. Moreover, the relations among topography, soil depth, soil moisture, transpiration rates and plant species' distribution at the hillslope scale can affect the soil water balance, defining spatial and temporal patterns (Tromp-van Meerveld and McDonnell, 2006). At the moment, this aspect is not included in the CRITERIA-3D model and the vegetation is allowed to have the same root maximum depth, canopy coverage and evapotranspiration activity everywhere inside the same land use domain. Including an heterogeneous soil depth and an heterogeneous vegetation presence or structure could help the stability simulations in being more accurate. Another aspect that will be further explored is the conceptual model of soil cracking behavior in relation to the different soil textural classes, based on field measurements.

7. Conclusions

In the presented research, the 3D agro-hydrological model CRITERIA-3D was extended and tested as a predictive tool for rainfall-induced shallow landslides involving transient modeling of vegetation effects on slope stability. Although designed for agronomic applications, results showed that the model is suitable for stability analyses in semi-natural environments. CRITERIA-3D is open-source, and researchers and practitioners can use it with any desired resolution, based on available DEMs. The model has been validated on a test slope where a shallow landslide occurred on 2nd March 2014, during a field monitoring campaign. Results showed that, although reducing the spatial resolution of the computational mesh, in this application the hydrology simulation outcomes did not significantly differ, neither for soil water content nor for soil water potential. However, an effect was observed in terms of slope stability, since the landslide occurrence was appropriately predicted only using a DEM Spatial resolution of 1 m, 2 m, and 5 m. The landslide prediction was satisfactory in terms of time.

The present research was related to a relatively small test area. The application of the proposed model to areas wider than a single slope are already ongoing.

CRediT authorship contribution statement

G. Sannino: Writing – original draft, Validation, Software, Methodology, Investigation, Conceptualization. **F. Tomei:** Validation, Software, Conceptualization. **M. Bittelli:** Software, Conceptualization. **C. Meisina:** Writing – review & editing, Data curation. **M. Bordoni:** Writing – review & editing, Data curation. **R. Valentino:** Writing – review & editing, Supervision, Project administration, Funding acquisition, Conceptualization.

Declaration of competing interest

The authors declare that they have no known competing financial interests or personal relationships that could have appeared to influence the work reported in this paper.

Data availability

Data will be made available on request.

References

Allen, R.G., Smith, M., Pereira, L.S., Perrier, A., 1994. An update for the calculation of reference evaporation. ICID Bulletin 43 (2), 35–92.

Anagnostopoulos, G.G., Fatichi, S., Burlando, P., 2015. An advanced process-based distributed model for the investigation of rainfall-induced landslides: the effect of process representation and boundary conditions. Water Resour. Res. 51 (9), 7501–7523.

Antolini, G., Tomei, F., Dottori, F., Marletto, V., Van Soetendael, M., Bittelli, M., 2016. CRITERIA technical manual. In: Arpae Emilia-Romagna - Hydro-Meteo-Climate Service. https://www.arpae.it/it/temi-ambientali/meteo/scopri-di-piu/strumenti-di-modellistica/criteria/criteria_2016_technical-manual.pdf. accessed 20 Oct 2024.

Arnone, E., Francipane, A., Dialynas, Y.G., Noto, L.V., Bras, R.L., 2021. Implications of terrain resolution on modeling rainfall-triggered landslides using a TIN-based model. Environ. Model Softw. 141, 105067.

Assouline, S., Or, D., 2006. Anisotropy factor of saturated and unsaturated soils. Water Resour. Res. 42 (12).

Bagarello, V., Sferlazza, S., Sgroi, A., 2009. Testing laboratory methods to determine the anisotropy of saturated hydraulic conductivity in a sandy–loam soil. Geoderma 154 (1–2), 52–58.

Baum, R.L., Savage, W.Z., Godt, J.W., 2008. TRIGRS – A FORTRAN Program for Transient Rainfall Infiltration and Grid-Based Regional Slope-Stability Analysis, Version 2.0: US Geological Survey Open-File Report 2008–1159 (81 pp).

Bittelli, M., Tomei, F., Pistocchi, A., Flury, M., Boll, J., Brooks, E.S., Antolini, G., 2010. Development and testing of a physically based, three-dimensional model of surface and subsurface hydrology. Adv. Water Resour. 33, 106–122.

Bogaard, T.A., Greco, R., 2016. Landslide hydrology: from hydrology to pore pressure. Wiley Interdiscip. Rev. Water 3 (3), 439–459.

Bordoni, M., Meisina, C., Valentino, R., Lu, N., Bittelli, M., Chersich, S., 2015. Hydrological factors affecting rainfall-induced shallow landslides: from the field monitoring to a simplified slope stability analysis. Eng. Geol. 193, 19–37.

Bordoni, M., Corradini, B., Lucchelli, L., Valentino, R., Bittelli, M., Vivaldi, V., Meisina, C., 2019. Empirical and physically based thresholds for the occurrence of shallow landslides in a prone area of Northern Italian Apennines. Water 11 (12), 2653.

Bordoni, M., Bittelli, M., Valentino, R., Vivaldi, V., Meisina, C., 2021. Observations on soil-atmosphere interactions after long-term monitoring at two sample sites subjected to shallow landslides. Bull. Eng. Geol. Environ. Open Access 2021. https://doi.org/10.1007/s10064-021-02334-y.

Brath, A., Casagli, N., Marani, M., Mercogliano, P., Motta, R., 2023. Rapporto della Commissione tecnico-scientifica istituita con deliberazione della Giunta Regionale n. 984/2023 e determinazione dirigenziale 14641/2023, al fine di analizzare gli eventi meteorologici estremi del mese di maggio 2023. Emilia-Romagna Region. https://www.regione.emilia-romagna.it/alluvione/rapporto-della-commissione-tecnico-scientifica/20231212_rapporto_commissione_rer.pdf/@@download/file (accessed 10 October 2024).

Brooks, E.S., 2003. Distributed Hydrologic Modeling of the Eastern Palouse (Doctoral dissertation,. University of Idaho.

Brooks, E.S., Boll, J., McDaniel, P.A., 2007. Distributed and integrated response of a geographic information system-based hydrologic model in the eastern Palouse region, Idaho. Hydrological Processes: Int. J. 21 (1), 110–122.

Casagrande, A., 1948. Classification and identification of soils. Trans. Am. Soc. Civ. Eng. 113 (1), 901–930.

Cheng, Q., Tang, C.S., Zeng, H., Zhu, C., An, N., Shi, B., 2020. Effects of microstructure on desiccation cracking of a compacted soil. Eng. Geol. 265, 105418.

Corominas, J., van Westen, C., Frattini, P., Cascini, L., Malet, J.P., Fotopoulou, S., Smith, J.T., 2014. Recommendations for the quantitative analysis of landslide risk. Bull. Eng. Geol. Environ. 73, 209–263.

Cotter, A.S., Chaubey, I., Costello, T.A., Soerens, T.S., Nelson, M.A., 2003. Water quality model output uncertainty as affected by spatial resolution of input data 1. JAWRA 39 (4), 977–986.

Doorenbos, J., Kassam, A., 1979. FAO Irrigation and Drainage Paper 33.

DiBiagio, A., Capobianco, V., Oen, A., Tallaksen, L.M., 2024. State-of-the-art: parametrization of hydrological and mechanical reinforcement effects of vegetation in slope stability models for shallow landslides. Landslides 21 (10), 2417–2446.

Ditzler, C., Scheffe, K., Monger, H.C., 2017. Soil Survey Manual. In: Soil Survey Division Staff; Soil Conservation Service Volume Handbook 18. U.S Department of Agriculture.

Driessen, P.M., Konijn, N.T., 1992. Land-Use Systems Analysis. WAU and Interdisciplinary Research (INRES).

Fernandes, N.F., Guimarães, R.F., Gomes, R.A., Vieira, B.C., Montgomery, D.R., Greenberg, H., 2004. Topographic controls of landslides in Rio de Janeiro: field evidence and modeling. Catena 55 (2), 163–181.

Fredlund, D.G., 1987. Slope stability analysis incorporating the effect of soil suction. Slope Stabi. 113–144.

Fredlund, D.G., Rahardjo, H., 1993. Soil Mechanics for Unsaturated Soils. John Wiley & Sons.

García-Gaines, R.A., Frankenstein, S., 2015. USCS and the USDA soil classification system: Development of a mapping scheme. https://vulcanhammer.net/wp-content/uploads/2019/10/p266001coll1_3757.pdf.

Godt, J.W., Şener-Kaya, B., Lu, N., Baum, R.L., 2012. Stability of infinite slopes under transient partially saturated seepage conditions. Water Resour. Res. 48 (5).

Gofar, N., Rahardjo, H., 2017. Saturated and unsaturated stability analysis of slope subjected to rainfall infiltration. In: MATEC Web of Conferences, vol. 101. EDP Sciences, p. 05004.

Gonzalez-Ollauri, A., Mickovski, S.B., 2017a. Hydrological effect of vegetation against rainfall-induced landslides. J. Hydrol. 549, 374–387.

Gonzalez-Ollauri, A., Mickovski, S.B., 2017b. Plant-soil reinforcement response under different soil hydrological regimes. Geoderma 285, 141–150.

Greco, R., Marino, P., Bogaard, T.A., 2023. Recent advancements of landslide hydrology. Wiley Interdiscip. Rev. Water 10 (6), e1675.

Guerra, E., Ventura, F., Snyder, R.L., 2016. Crop coefficients: a literature review. J. Irrig. Drain. Eng. 142 (3), 06015006.

Guzzetti, F., Carrara, A., Cardinali, M., Reichenbach, P., 1999. Landslide hazard evaluation: a review of current techniques and their application in a multi-scale study, Central Italy. Geomorphology 31 (1–4), 181–216.

Guzzetti, F., Gariano, S.L., Peruccacci, S., Brunetti, M.T., Marchesini, I., Rossi, M., Melillo, M., 2020. Geographical landslide early warning systems. Earth Sci. Rev. 200, 102973.

Hagedorn, F., Bundt, M., 2002. The age of preferential flow paths. Geoderma 108 (1–2), 119–132.

Hardy, R.J., Bates, P.D., Anderson, M.G., 1999. The importance of spatial resolution in hydraulic models for floodplain environments. J. Hydrol. 216 (1–2), 124–136.

Hong, Y., Adler, R., Huffman, G., 2006. Evaluation of the potential of NASA multi-satellite precipitation analysis in global landslide hazard assessment. Geophys. Res. Lett. 33 (22).

Hwang, I.T., Park, H.J., Lee, J.H., 2023. Probabilistic analysis of rainfall-induced shallow landslide susceptibility using a physically based model and the bootstrap method. Landslides 20 (4), 829–844.

IPCC, 2023. In: Core writing Team, Lee, H., Romero, J. (Eds.), Climate Change 2023: Synthesis Report. Contribution of Working groups I, II and III to the Sixth Assessment Report of the Intergovernmental Panel on climate Change. IPCC, Geneva, Switzerland, pp. 35–115. https://doi.org/10.59327/IPCC/AR6-9789291691647.

Ippisch, O., Vogel, H.J., Bastian, P., 2006. Validity limits for the van Genuchten–Mualem model and implications for parameter estimation and numerical simulation. Adv. Water Resour. 29 (12), 1780–1789.

Kellogg, C.E., 1937. Soil survey manual (no 274). In: US Department of Agriculture. Soil Survey Division Staff; Soil Conservation Service Volume Handbook 18. U.S Department of Agriculture.

Krisnanto, S., Rahardjo, H., Fredlund, D.G., Leong, E.C., 2014. Mapping of cracked soils and lateral water flow characteristics through a network of cracks. Eng. Geol. 172, 12–25.

Lepore, C., Arnone, E., Noto, L.V., Sivandran, G., Bras, R.L., 2013. Physically based modeling of rainfall-triggered landslides: a case study in the Luquillo forest, Puerto Rico. Hydrol. Earth Syst. Sci. 17 (9), 3371–3387.

Li, J.H., Zhang, L.M., 2011. Study of desiccation crack initiation and development at ground surface. Eng. Geol. 123 (4), 347–358.

Li, J.H., Zhang, L.M., Li, X., 2011. Soil-water characteristic curve and permeability function for unsaturated cracked soil. Can. Geotech. J. 48 (7), 1010–1031.

Liston, G.E., Sturm, M., 1998. A snow-transport model for complex terrain. J. Glaciol. 44 (148), 498–516.

Liu, X., Lan, H., Li, L., Cui, P., 2022. An ecological indicator system for shallow landslide analysis. Catena 214, 106211.

Lu, N., Godt, J., 2008. Infinite slope stability under steady unsaturated seepage conditions. Water Resour. Res. 44 (11).

Luo, Y., Zhang, J., Zhou, Z., Aguilar-Lopez, J.P., Greco, R., Bogaard, T., 2023. Effects of dynamic changes of desiccation cracks on preferential flow: experimental investigation and numerical modeling. Hydrol. Earth Syst. Sci. 27 (3), 783–808.

Martin, P., 1993. Vegetation responses and feedbacks to climate: a review of models and processes. Clim. Dyn. 8 (4), 201–210.

Masi, E.B., Tofani, V., Rossi, G., Cuomo, S., Wu, W., Salciarini, D., Catani, F., 2023. Effects of roots cohesion on regional distributed slope stability modelling. Catena 222, 106853.

McMaster, G.S., Wilhelm, W.W., 1997. Growing degree-days: one equation, two interpretations. Agric. For. Meteorol. 87 (4), 291–300.

Meena, V., Kumari, S., Shankar, V., 2022. Physically based modelling techniques for landslide susceptibility analysis: a comparison. IOP Conf Ser Earth Environ Sci 1032 (012033), 1.

Mualem, Y., 1976. A new model for predicting the hydraulic conductivity of unsaturated porous media. Water Resourc. Res. 12 (3), 513–522.

Mualem, Y., 1984. Anisotropy of unsaturated soils. Soil Sci. Soc. Am. J. 48 (3), 505–509.

Murgia, I., Giadrossich, F., Mao, Z., Cohen, D., Capra, G.F., Schwarz, M., 2022. Modeling shallow landslides and root reinforcement: a review. Ecol. Eng. 181, 106671.

Olivares, L., Damiano, E., Mercogliano, P., Picarelli, L., Netti, N., Schiano, P., Manzi, M. P., 2014. A simulation chain for early prediction of rainfall-induced landslides. Landslides 11, 765–777.

Oliveira, S.C., Zêzere, J.L., Lajas, S., Melo, R., 2017. Combination of statistical and physically based methods to assess shallow slide susceptibility at the basin scale. Nat. Hazards Earth Syst. Sci. 17 (7), 1091–1109.

Papa, M.N., Medina, V., Ciervo, F., Bateman, A., 2013. Derivation of critical rainfall thresholds for shallow landslides as a tool for debris flow early warning systems. Hydrol. Earth Syst. Sci. 17 (10), 4095–4107.

Park, J.Y., Lee, S.R., Lee, D.H., Kim, Y.T., Lee, J.S., 2019. A regional-scale landslide early warning methodology applying statistical and physically based approaches in sequence. Eng. Geol. 260, 105193.

Peron, H., Hueckel, T., Laloui, L., Hu, L., 2009. Fundamentals of desiccation cracking of fine-grained soils: experimental characterisation and mechanisms identification. Can. Geotech. J. 46 (10), 1177–1201.
Persichillo, M.G., Bordoni, M., Meisina, C., 2017. The role of land use changes in the distribution of shallow landslides. Sci. Total Environ. 574, 924–937.
Petersen, C.T., Trautner, A., Hansen, S., 2008. Spatio-temporal variation of anisotropy of saturated hydraulic conductivity in a tilled sandy loam soil. Soil Tillage Res. 100 (1–2), 108–113.
Reichenbach, P., Rossi, M., Malamud, B.D., Mihir, M., Guzzetti, F., 2018. A review of statistically-based landslide susceptibility models. Earth Sci. Rev. 180, 60–91.
Rigon, R., Bertoldi, G., Over, T.M., 2006. GEOtop: a distributed hydrological model with coupled water and energy budgets. J. Hydrometeorol. 7 (3), 371–388.
Ritchie, J.T., Nesmith, D.S., 1991. Temperature and crop development. Model. Plant Soil Syst. 31, 5–29.
Safari, E., Ghazizade, M.J., Abduli, M.A., Gatmiri, B., 2014. Variation of crack intensity factor in three compacted clay liners exposed to annual cycle of atmospheric conditions with and without geotextile cover. Waste Manag. 34 (8), 1408–1415.
Safari, E., Ghazizade, M.J., Abduli, M.A., Gatmiri, B., 2014. Variation of crack intensity factor in three compacted clay liners exposed to annual cycle of atmospheric conditions with and without geotextile cover. Waste Manage. 34 (8), 1408–1415.
Sannino, G., Tomei, F., Bittelli, M., Bordoni, M., Meisina, C., Valentino, R., 2024. Implementation of a slope stability method in the CRITERIA-1D agro-hydrological modeling scheme. Landslides 1–20.
Schoorl, J.M., Sonneveld, M.P.W., Veldkamp, A., 2000. Three-dimensional landscape process modelling: the effect of DEM resolution. Earth Surface Proces. Landf. J. British Geomorphological Research Group 25 (9), 1025–1034.
Simoni, S., Zanotti, F., Bertoldi, G., Rigon, R., 2008. Modelling the probability of occurrence of shallow landslides and channelized debris flows using GEOtop-FS. Hydrological Processes: Int. J. 22 (4), 532–545.
Stewart, R.D., Najm, M.R.A., 2020. Field measurements of soil cracks. Soil Sci. Soc. Am. J. 84 (5), 1462–1476.
Tang, C.S., Shi, B., Liu, C., Gao, L., Inyang, H.I., 2011. Experimental investigation of the desiccation cracking behavior of soil layers during drying. J. Mater. Civ. Eng. 23 (6), 873–878.
Tang, C.S., Zhu, C., Cheng, Q., Zeng, H., Xu, J.J., Tian, B.G., Shi, B., 2021. Desiccation cracking of soils: a review of investigation approaches, underlying mechanisms, and influencing factors. Earth Sci. Rev. 216, 103586.
Tarolli, P., Dalla Fontana, G., 2009. Hillslope-to-valley transition morphology: New opportunities from high resolution DTMs. Geomorphology 113 (1–2), 47–56.
Tiranti, D., Rabuffetti, D., 2010. Estimation of rainfall thresholds triggering shallow landslides for an operational warning system implementation. Landslides 7, 471–481.
Toll, D.G., Lourenço, S.D.N., Mendes, J., Gallipoli, D., Evans, F.D., Augarde, C.E., Tarantino, A., 2011, February. Soil Suction Monitoring For Landslides and Slopes. Geological Society of London.
Tomei, F., Antolini, G., Villani, G., Bittelli, M., Sannino, G., 2024. CRITERIA-1D Technical Manual. https://github.com/ARPA-SIMC/CRITERIA1D/blob/master/DOC/CRITERIA1D_technical_manual.pdf.
Trabelsi, H., Chebbi, M., Guiras, H., Jamei, M., Romero Morales, E.E., 2018. Stabilization of clayey soil using fibre reinforcement. In: Unsaturated Soils: UNSAT 2018: The 7th International Conference on Unsaturated Soils. The Hong Kong University of Science and Technology (HKUST), pp. 545–550.
Tromp-van Meerveld, H.J., McDonnell, J.J., 2006. On the interrelations between topography, soil depth, soil moisture, transpiration rates and species distribution at the hillslope scale. Adv. Water Resour. 29 (2), 293–310.
Trudgill, D., Honek, A.D.L.I., Li, D., van Straalen, N.M., 2005. Thermal time–concepts and utility. Ann. Appl. Biol. 146 (1), 1–14.
Van Dam, J.C., Feddes, R.A., 2000. Numerical simulation of infiltration, evaporation and shallow groundwater levels with the Richards equation. J. Hydrol. 233 (1–4), 72–85.
Viet, T.T., Lee, G., Thu, T.M., An, H.U., 2017. Effect of digital elevation model resolution on shallow landslide modeling using TRIGRS. Nat. Haz. Rev. 18 (2), 04016011.
Wardhana, I.W., Budihardjo, M.A., Istirokhatun, T., Ikhlas, N., 2021, November. Desiccation cracks behaviour of leachate in bentonite-zeolite composite liner. In: IOP Conference Series: Earth and Environmental Science, vol. 894, No. 1. IOP Publishing, p. 012043.
Wypych, A., Sulikowska, A., Ustrnul, Z., Czekierda, D., 2017. Variability of growing degree days in Poland in response to ongoing climate changes in Europe. Int. J. Biometeorol. 61, 49–59.
Yesiller, N., Miller, C.J., Inci, G., Yaldo, K., 2000. Desiccation and cracking behavior of three compacted landfill liner soils. Eng. Geol. 57 (1–2), 105–121.
Young, I.M., Crawford, J.W., Rappoldt, C., 2001. New methods and models for characterising structural heterogeneity of soil. Soil Tillage Res. 61 (1–2), 33–45.
Yuan-Shu, J.I.N.G., Zhang, B., Thimm, A., Zepp, H., 2008. Anisotropy of soil hydraulic properties along arable slopes. Pedosphere 18 (3), 353–362.
Zhang, J.M., Luo, Y., Zhou, Z., Chong, L., Victor, C., Zhang, Y.F., 2021. Effects of preferential flow induced by desiccation cracks on slope stability. Eng. Geol. 288, 106164.
Zhang, J., Qiu, H., Tang, B., Yang, D., Liu, Y., Liu, Z., Zhu, Y., 2022. Accelerating effect of vegetation on the instability of rainfall-induced shallow landslides. Remote Sens. 14 (22), 5743.
Zuo, X., Zhao, X., Zhao, H., Zhang, T., Guo, Y., Li, Y., Huang, Y., 2009. Spatial heterogeneity of soil properties and vegetation–soil relationships following vegetation restoration of mobile dunes in Horqin Sandy Land, Northern China. Plant Soil 318, 153–167.